A Two-Dimensional Lagrangean Code for
Laser-Produced Plasma Applications.
Pt.1. Crater Formation in Plane Targets

L.L. Lengyel

MAX-PLANCK-INSTITUT FÜR PLASMAPHYSIK

GARCHING BEI MÜNCHEN

MAX-PLANCK-INSTITUT FÜR PLASMAPHYSIK

GARCHING BEI MÜNCHEN

A Two-Dimensional Lagrangean Code for
Laser-Produced Plasma Applications.
Pt.1. Crater Formation in Plane Targets

L.L. Lengyel

IPP 4/135   November 1975

IPP 4/135

A Two-Dimensional Lagrangean
Code for Laser-Produced Plasma
Applications. Pt. 1. Crater
Formation in Plane Targets

L.L. Lengyel

November 1975

Abstract

A two-dimensional Lagrangean hydrodynamic code has been
developed for laser-produced plasma applications. In
testing the hydrodynamic part of the code the irradiation
of thin foils with high-intensity laser beams was
considered in a single-fluid single-temperature
approximation. The computed shock velocities, compression
ratios, velocity and pressure variations, etc. are in
good agreement with estimates stemming from analytical
solutions.

INTRODUCTION

The heating of solid, liquid, or gaseous targets by means
of lasers is characterized by the presence of rather
large spatial gradients in the substance interacting
with the laser light. In the case of unshaped laser
pulses the plasma parameters may vary by four or five
orders of magnitude over distances not exceeding a few
per cent of the characteristic length involved. Still
larger are the spatial gradients if specially shaped
laser pulses are used as, for example, in the case of
compression by coalescing waves, etc. The use of
Lagrangean hydrodynamic codes, which are particularly
well suited to handling large gradients with one spatial
dimension, is most common in such cases (see, for
example, Kidder and Barnes [1], Clarke et al. [2],
Christiansen et al. [3], Goldman [4], Lengyel [5], or
the sources cited in the review paper of Mulser et al.
[6]). The assumption of strict symmetry (slab, cylindrical,
or spherical symmetry) is mandatory in claculations of
this kind.

However, in the majority of cases that can be realized
experimentally the boundary conditions are nonuniform
and thus the application of more sophisticated numerical
models becomes necessary. In some cases the existence
of certain uniformity or symmetry properties allows the
use of two-dimensional (2D) codes for modeling the
problem. When plasma production by laser is considered,
the assumption of axial symmetry may be a good approxi-
mation for numerous experimental situations (irradiation
of plane surfaces or targets with rotational symmetry
by a single cylindrically symmetric laser beam, double-
sided coaxial irradiation of sheaths or rotationally
symmetric targets, etc.). Note, however, that if a
magnetic field is present, axial symmetry only exists if

the magnetic field is linear, rotationally symmetric and
the target is irradiated along the magnetic field lines
(beam axis coincides with the magnetic axis).

The question that may naturally arise is how well is a
Lagrangean mass-cell system suited to handling truly
two-dimensional problems, i.e. problems in which not only
deviations from one-dimensional symmetry conditions are
being considered. Most of the results published on 2D
Lagrangean laser-induced fusion calculations are con-
cerned with the destabilizing effects caused by deviations
from 1D symmetry conditions (see, for example, [7]).
Besides, no information at all has been available until
recently on the details of 2D Lagrangean codes as applied
to laser-rpoduced plasma calculations (see, for example,
[7],[8] or, more recently, [9]). Two-dimensional calculations
have also been performed in Los Alamos [10] (a PIC code,
the results are also described in [6]). A 2D ADI method
based on a fixed-grid Eulerian system has been developed
by Lindemuth [11]. It should be noted here that neither
the particle-in-cell (PIC) method nor a fixed-grid Eulerian
system seem to be particularly well suited to handling
the extreme gradients inherent in laser-produced plasmas.

It was thus decided some time ago to develop a 2D Lagrangean
hydrodynamic code [12] and test its applicability to
axially-symmetric laser-produced plasma calculations with
and without magnetic fields present. Some results obtained
during the test runs and pertaining to the burn-through
of deuterium ice layers irradiated from one side by single
laser beams in the absence of magnetic fields are reported
here.

MATHEMATICAL MODEL

An excellent treatise on 2D Lagrangean hydrodynamic
calculations was written by Schulz [13]. Readers
interested in details concerning the formulation of a
generalized 2D Lagrangean coordinate system and the
discretization of the conservation equations in the
coordinate system thus defined are referred to [13].
Schulz also indicated some of the difficulties one may
encounter while working with 2D Lagrangean codes (see
the computational example provided by him). Since the
computer code used in the present calculations closely
follows the method presented in [13], we shall omit here
the lengthy derivations and only outline the major
modifications introduced in Schulz's original system
(see also [14]).

The conservation equations are written in a one-
temperature ideal gas approximation:

$$\frac{\partial \rho}{\partial t} + \nabla \cdot (\rho \vec{u}) = 0 \quad , \tag{1.1}$$

$$\rho \left(\frac{\partial}{\partial t} + \vec{u} \cdot \nabla \right) \vec{u} = - \nabla \mathbb{P} \quad , \tag{1.2}$$

$$\rho \left(\frac{\partial}{\partial t} + \vec{u} \cdot \nabla \right) e = - \nabla \cdot \vec{\phi}_\ell - \mathbb{P} \nabla \cdot \vec{u} \quad , \tag{1.3}$$

where $\mathbb{P} = p + q$ and

$$e = \frac{1}{\gamma - 1} \frac{p}{\rho} \tag{1.4}$$

The symbols q and $\vec{\phi}_\ell$ represent artificial viscosity and
laser flux intensity, respectively. Introducing a pair
of generalized curvelinear coordinates a, b and defining
a vector $\vec{s}$ by a clock-wise rotation of the radius vector
$\vec{r}$ over an angle of $\pi/2$, the transformation formulae from
the old cylindrical coordinate system (r, z) to the new
curvilinear one (a, b) may be written as follows:

$$\text{grad } f = \frac{1}{J}\left(\frac{\partial \vec{s}}{\partial b}\frac{\partial}{\partial a} - \frac{\partial \vec{s}}{\partial a}\frac{\partial}{\partial b}\right)f =$$

$$= \frac{1}{J}\left[\hat{r}\left(\frac{\partial z}{\partial b}\frac{\partial}{\partial a} - \frac{\partial z}{\partial a}\frac{\partial}{\partial b}\right) - \hat{z}\left(\frac{\partial r}{\partial b}\frac{\partial}{\partial a} - \frac{\partial r}{\partial a}\frac{\partial}{\partial b}\right)\right]f \qquad (1.5)$$

$$\text{div } \vec{f} = \frac{1}{J}\left(\frac{\partial \vec{s}}{\partial b}\cdot\frac{\partial}{\partial a} - \frac{\partial \vec{s}}{\partial a}\cdot\frac{\partial}{\partial b}\right)\vec{f} =$$

$$= \frac{1}{J}\left(\frac{\partial z}{\partial b}\frac{\partial}{\partial a} - \frac{\partial z}{\partial a}\frac{\partial}{\partial b}\right)f_r - \frac{1}{J}\left(\frac{\partial r}{\partial b}\frac{\partial}{\partial a} - \frac{\partial r}{\partial a}\frac{\partial}{\partial b}\right)f_z \qquad (1.6)$$

where
$$J \equiv \partial(\vec{r},z)/\partial(b,a) = \frac{\partial r}{\partial a}\cdot\frac{\partial z}{\partial b} - \frac{\partial r}{\partial b}\cdot\frac{\partial z}{\partial a} \qquad (1.7)$$

and
$$\vec{r} = (r,z) \quad , \quad \vec{\lambda} = (-z, r) . \qquad (1.8)$$

Applying the transformation to the conservation equations
we obtain the following set of Lagrangean equations:

$$\rho r J = \text{const} = m , \qquad (1.9)$$

$$\frac{\partial \vec{u}}{\partial t} = -\frac{r}{m}\left(\vec{\lambda}_b \frac{\partial p}{\partial a} - \vec{\lambda}_a \frac{\partial p}{\partial b} + \vec{\lambda}_b \frac{\partial q_A}{\partial a} - \vec{\lambda}_a \frac{\partial q_B}{\partial b}\right), \qquad (1.10)$$

$$\frac{\partial \vec{r}}{\partial t} = \vec{u} , \qquad (1.11)$$

$$V = 1/\rho = \frac{r}{m}J , \qquad (1.12)$$

$$\frac{\partial e}{\partial t} = -\nabla\cdot\vec{\phi}_\ell - p\frac{\partial V}{\partial t} - \frac{q_A}{m}\frac{\partial}{\partial a}\left(r\vec{\lambda}_b\cdot\vec{u}\right) + \frac{q_B}{m}\frac{\partial}{\partial b}\left(r\vec{\lambda}_a\cdot\vec{u}\right). \qquad (1.13)$$

The rate of change of the total energy per unit mass is
given by

$$\frac{\partial}{\partial t}\left(\frac{u^2}{2} + e\right) = -\nabla\cdot\vec{\phi}_\ell - p\frac{\partial V}{\partial t} - \frac{1}{m}\frac{\partial}{\partial a}\left[(p+q_A)r\vec{\lambda}_b\cdot\vec{u}\right] +$$

$$+ \frac{1}{m}\frac{\partial}{\partial b}\left[(p+q_B)r\vec{\lambda}_a\cdot\vec{u}\right] . \qquad (1.14)$$

In the above expressions, the subscripts of $\vec{s}$ denote
derivatives with respect to the coordinates indicated.
As one may notice, the scalar artificial viscosity q

appearing in eqs. (1.2) and (1.3) has been replaced by a
tensor artificial viscosity $\bar{\bar{q}}$ appearing in eqs. (1.10) to
(1.14), which is characterized by the following relations:

$$q_A \neq 0 \quad \text{only if} \quad \partial \vec{u}/\partial a \neq 0 \quad ,$$

$$q_B \neq 0 \quad \text{only if} \quad \partial \vec{u}/\partial b \neq 0 \quad . \tag{1.15}$$

Such a definition of $\bar{\bar{q}}$ is necessary for assuring the
continuity of the velocity component parallel to a shock
front (only the normal component should be affected by the
artificial viscosity). In general, q_A and q_B may be
specified as functions of the respective velocity gradients.
Schulz used the product of the first and second derivatives
of the velocity components for defining q_A and q_B. Such an
approximation seemed tedious and rather approximate at the
boundaries of the region occupied by the fluid owing to
the difficulties associated with the discretization of
second derivatives in generalized coordinates at a fluid-
-vacuum interface. Hence only combinations of the first
derivatives were used for defining $\bar{\bar{q}}$ in the present
computations. The resulting numerical system functioned
well also with rather large cell deformations.

Note that equations (1.10) and (1.13) differ from the
respective equations of Schulz. Splitting the artificial
viscosity into individual constituents, i.e. the arbitrary
replacement of a scalar quantity by a tensor one has the
undesired effect that eq. (1.13) is no longer invariant
with respect to Galilean transformation, i.e. it is no
longer an exact analogue of eq. (1.3). For preserving
the invariance of the energy equation with respect to
Galilean transformation Schulz changed simultanesouly
the structures of eqs. (1.10) and (1.13) in a rather
arbitrary manner, but still conserving the total energy
per unit mass, i.e. leaving eq. (1.14) unchanged. Following

Schulz, eqs. (1.10) and (1.13) should be written in the following form:

$$\frac{\partial \vec{u}}{\partial t} = -\frac{t}{m}\left(\vec{\lambda}_b^2 \frac{\partial p}{\partial a} - \lambda_a \frac{\partial p}{\partial b}\right) - \frac{1}{m}\left[\frac{\partial}{\partial a}\left(q_A + \vec{\lambda}_b\right) - \frac{\partial}{\partial b}\left(q_B + \vec{\lambda}_a\right)\right] \, , \quad (1.16)$$

$$\frac{\partial e}{\partial t} = -\nabla \cdot \vec{\phi}_\ell - p\frac{\partial V}{\partial t} - \frac{t}{m}\left(q_A \vec{\lambda}_b \cdot \frac{\partial \vec{u}}{\partial a} - q_B \vec{\lambda}_a \cdot \frac{\partial \vec{u}}{\partial b}\right) . \quad (1.17)$$

In this representation, the invariance of the energy equation is assured.

For the sake of clarity, computations were performed following both approaches, i.e. by means of eqs. (1.10) to (1.13) as well as by eqs. (1.16) to (1.17). The results were found to be qualitatively about the same in both cases (the shape of the expanding gas cloud, the form of the crater developing in the ice layer, etc.), but the quantitative difference between the local gas parameter values amounted to 25 % to 30 % in some cases. Since, as shall be seen, the application of eqs. (1.10) and (1.13) yielded results that are in good agreement with theoretical predictions, it has been decided to use these equations irrespective of their Galilean trans-formation properties.

In the computations described here 100 % laser energy damping was assumed to take place at a particular gas density value, i.e. in the last mass-cell whose density is just below a given threshold value (following the direction of propagation of the laser light). In most of the calculations this threshold value was defined in terms of the electron density at which the laser beam frequency is equal to the electron plasma frequency, i.e. $\omega_\ell = \omega_p = \left(n_e e^2 / m_e \varepsilon_0\right)^{1/2}$. In a fully ionized deuterium plasma, the electron density may then be replaced by the respective gas density, i.e. $n_e = \varrho / m_D$. In the case of deuterium gas, $\varrho_{crit}/\varrho_0 \approx 1/50$, where ϱ_0 denotes

deuterium ice density ($\varrho_0 \approx 0.196$ gr/cm^3, measured value
[15]). Such an approach made it rather simple to discretize
the term $\nabla \cdot \vec{\phi}_\varrho$ appearing in the energy equation.

In a series of calculations performed, allowance was made
for heat conduction, i.e. the term

$$-\nabla \cdot \vec{\phi}_{cond} = Const \cdot div\left(\mathcal{H}\, grad\, e\right) \;,\; \mathcal{H} \propto e^{5/2} \qquad (1.18)$$

has been introduced into the energy equation. Owing to
the temperature-dependence of $\mathcal{H}$, heat conduction was found
to affect primarily the high-temperature expansion fan of
the gas blob produced: at sufficiently high laser flux
intensities the expansion fan became nearly isothermal.
In the low-temperature shock-heated gas region ahead of
the absorption zone the conduction effect was found to be
negligible.

Note that in view of eqs. (1.5) and (1.6) the right-hand
side of eq. (1.18) consists of eight second-order
derivatives, four of them being of the mixed-type. The
recurrence formula for the internal energy of a particular
mass-cell contains terms with the internal energies of the
eight adjacent cells. In view of the temperature-dependence
of the thermal conductivity the finite difference version
of this equation can only be solved by means of rather
crude approximations. In the present calculations, an
explicit time-splitting scheme was used and the temperature-
-dependence of $\mathcal{H}$ was accounted for by an iterative
procedure. Since the computer time required for such a
solution was found to be rather long and the yield rather
low (the distributions computed with and without thermal
conduction showed no other difference than the one described
above) it was decided to abandon thermal diffusion until a
more effective way of computing it is found.

RESULTS

A deuterium ice layer of thickness l_0/ℓ, density ρ_0, and temperature T_0 was heated by a cylindrical laser beam whose diameter was equal to the ice thickness: $D\ell = l_0/\ell$. The radial (lateral) dimension of the target-layer R_0 was chosen so as to assure complete burn-through before the bow shock reaches the lateral side of the ice layer. The ratio $R_0/l_0 = 2/1$ was found to be satisfactory in most of the computational cases considered. For simulating absorption at a certain "critical" density value, an expansion fan was attached to the side of the ice layer exposed to the laser beam. The thickness of this layer was l_0/ℓ as well. The density was assumed to vary cubically in the expansion fan from zero to ρ_0. The initial parameter values were selected to correspond to measured data: $\rho_0 = 0.196$ gr/cm^3, and $c_0 \approx 2 \times 10^5$ cm/sec (density and sonic velocity in deuterium ice [14]). Hence assuming a total ice thickness of $l_0 = 200\ \mu$ the characteristic time associated with the propagation of sonic disturbance over l_0 is $\tau_0 = 100$ ns. The dimensionless times dispalyed in the plots that follows are given in fractions of this time (all computations were performed in dimensionless coordinates by means of reduced variables). The dimensionless quantity Q^* appearing in the figures is related to the laser flux ϕ_ℓ by means of the expression $Q^* = \gamma(\gamma-1)(l_0/\Delta_{absrb})(\rho_0/\rho_{crit})\phi_\ell/\phi_0$, where $\phi_0 = \rho_0 c_0^3$ and Δ_{absrb} denotes the "absorption length". Note that different combinations of initial values may yield the same input parameter Q^*.

The plots shown in Fig. 1 correspond to $\phi_\ell = 5 \times 10^{12}$ W/cm^2 and $t_{pulse} = 200$ ps. The pictures in the left-side column show the cell deformation, i.e. the development of a shock wave in the undisturbed material, and the rapid expansion of the gas cloud on the vacuum-side of the surface irradiated. The plots in the right-side column are vector plots
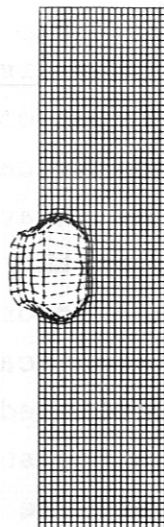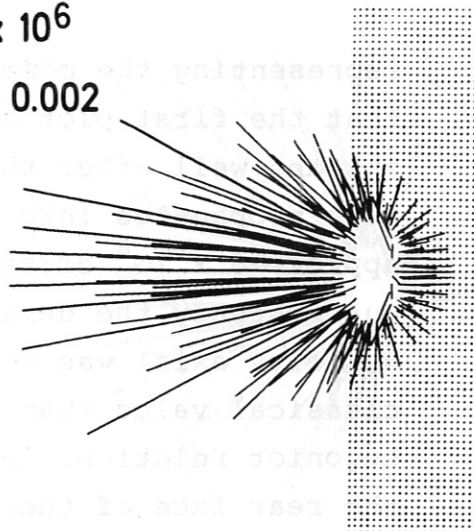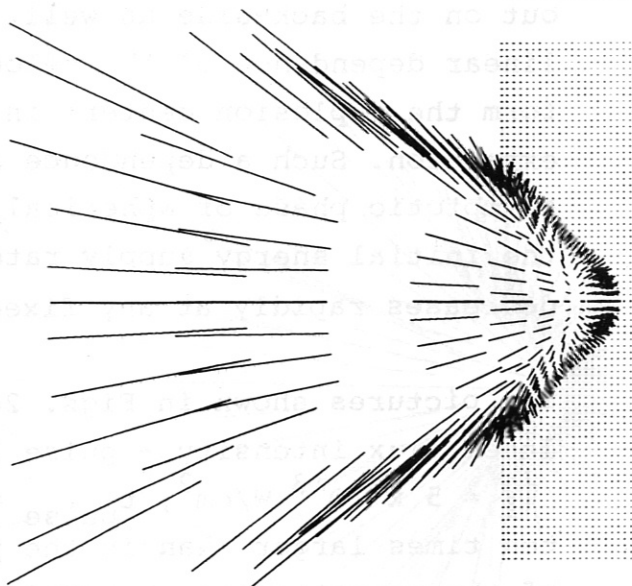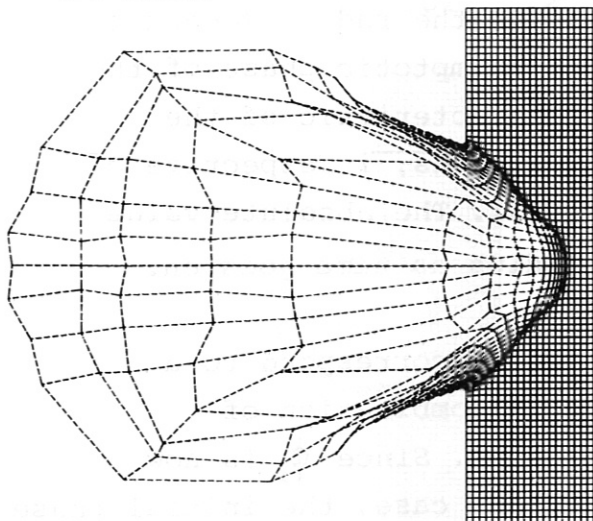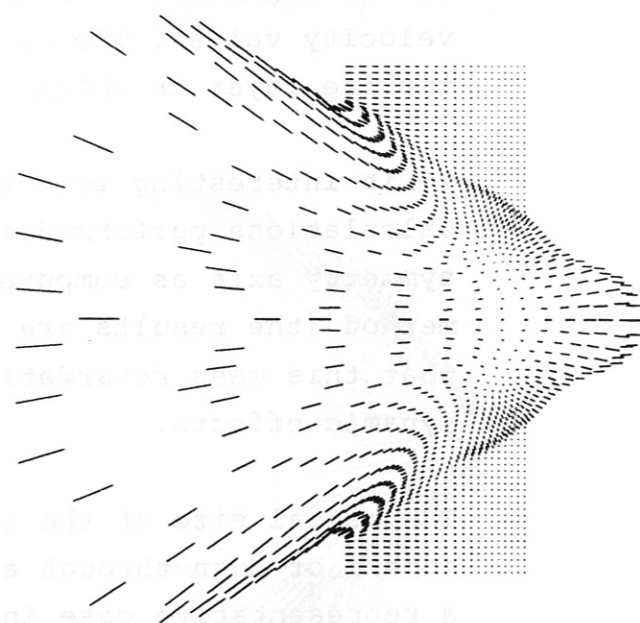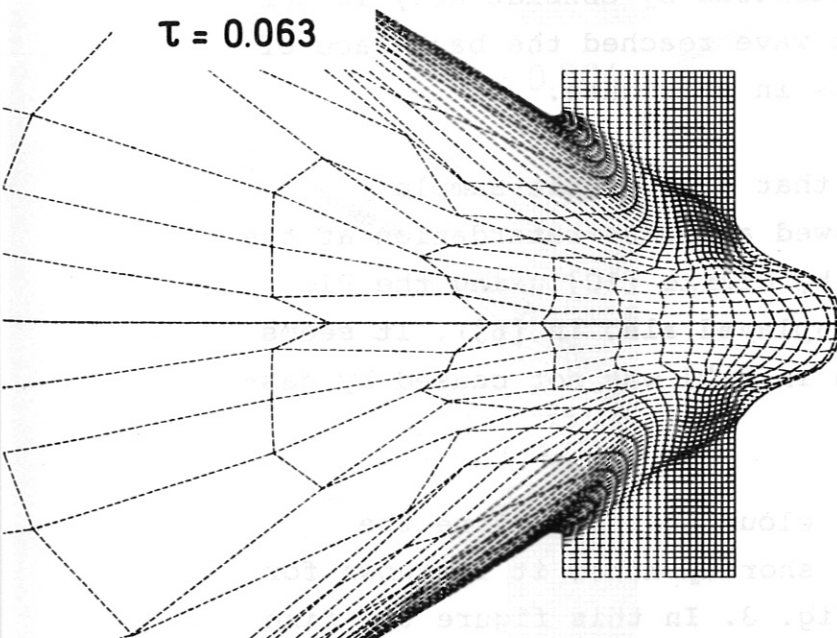
Fig. 1   Crater formation in a deuterium ice layer.
$\phi_\ell = 5 \times 10^{12}$ W/cm^2, $t_{pulse} = 200$ ns.
(Q, τ - dimensionless quantities, $\tau_0 = 100$ ns).

representing the momentary velocity distributions. Note
that the first plot displayed corresponds to a time
instant well after the pulse end. As can be seen, a shock
wave propagates into the solid at an average velocity of
approx. 5×10^6 cm/sec. As long as the shock wave remained
quasi-steady the density increase across it (along the
symmetry axis) was found to be identical with the
classical value that could be predicted from the Rankine-
Hugoniot relation. In about 5 ns the shock wave reaches
the rear face of the ice layer and the gas starts to stream
out on the back-side as well. Note the approximately
linear dependence of the velocity on the radius (measured
form the explosion center) in the asymptotic phase of the
expansion. Such a dependence is characteristic of the
asymptotic phase of spherical expansions, irrespective of
the initial energy supply rates [16]. The absolute value
decreases rapidly at any fixed radius as time goes on.

The pictures shown in Figs. 2a and 2b correspond to a
laser flux intensity - pulse length combination of
$\phi_\ell = 5 \times 10^{13}$ W/cm^2, t_{pulse} = 100 ps. Since ϕ_ℓ is now
ten times larger than in the previous case, the initial phase
of the expansion is characterized by considerably larger
velocity values. The shock wave reached the back-face of
the ice layer in about 2 ns in this case.

It is interesting to note that none of the sample
calculations performed showed any mass-retardation at the
symmetry axis as computed by Clarke [10] using the PIC
method (the results are displayed also in [6]). It seems
that this mass retardation in [10] was not caused by gas-
dynamic effects.

The actual size of the gas cloud shortly before the
moment of burn-through and shortly after it is shown for
a representative case in Fig. 3. In this figure the fine
structures of the respective craters are also given (the
plot-scale has been changed). Note the good stability of
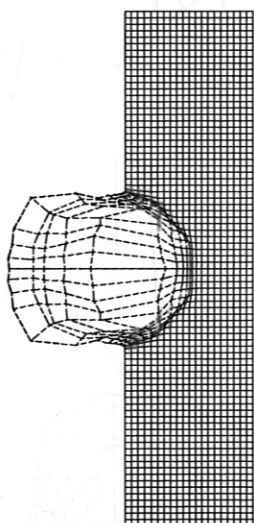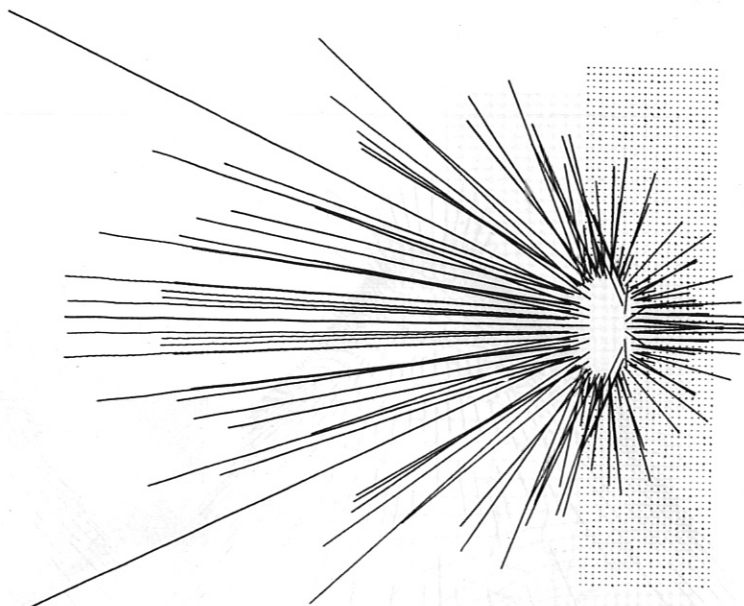the numerical system also at the relatively large cell
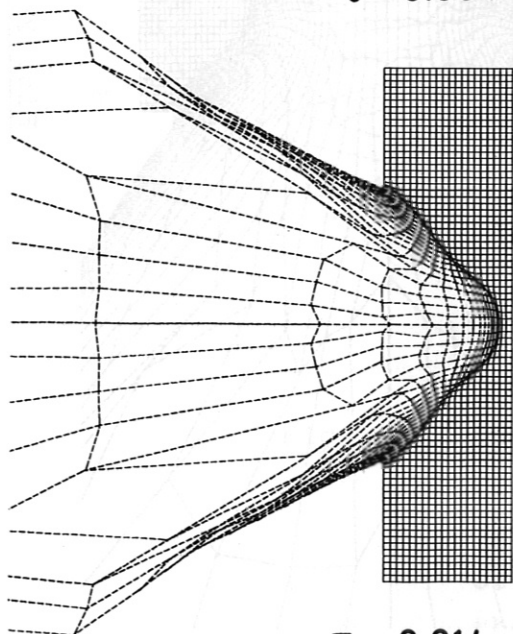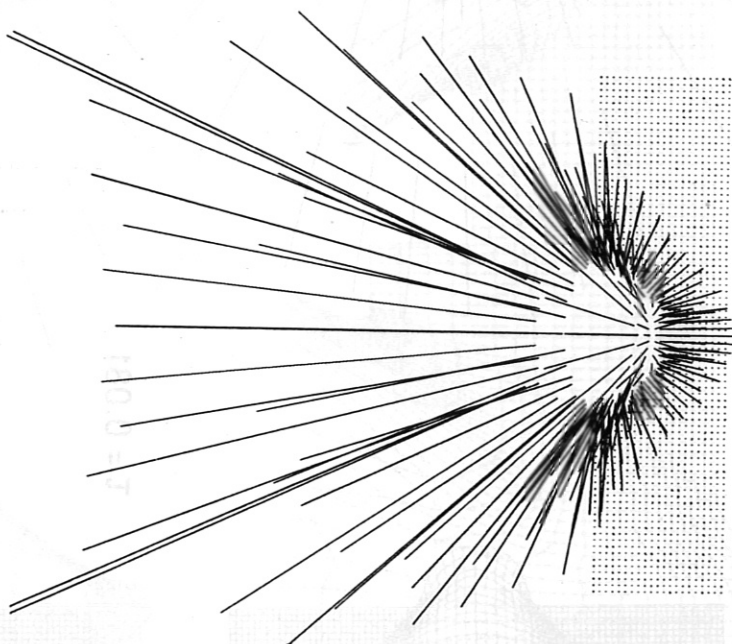deformations observed.

$Q^* = 4 \times 10^7$

$\tau_{pulse} = 0.001$
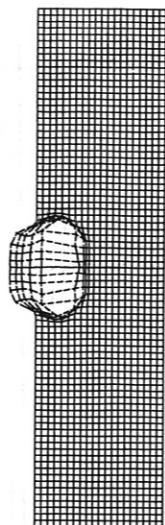
$\tau = 0.002$

$\tau = 0.004$

$\tau = 0.014$
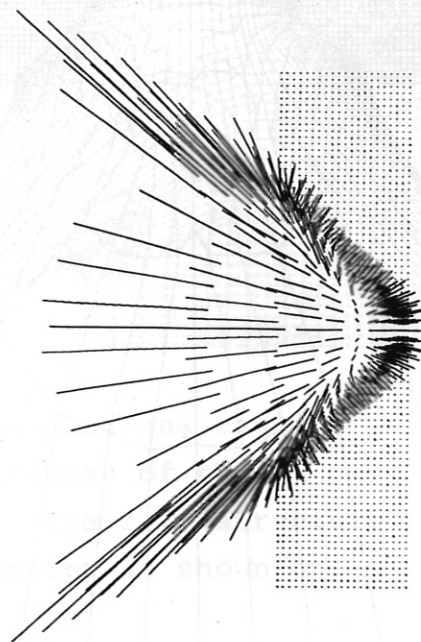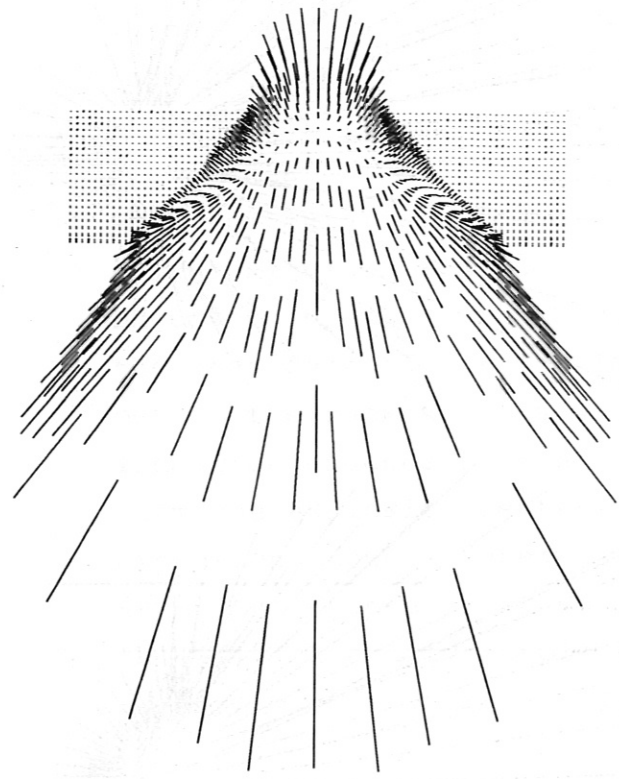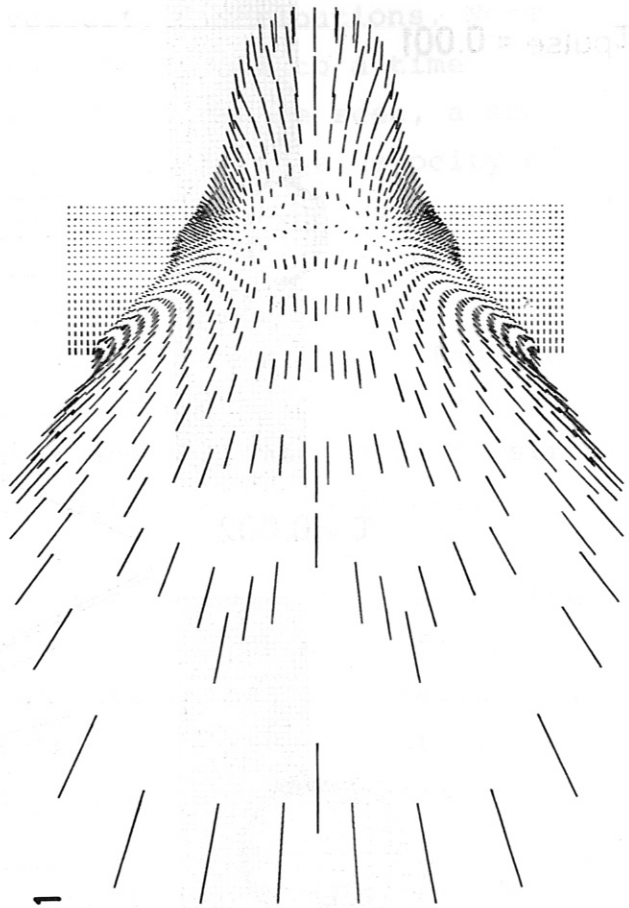
Fig. 2a   Crater formation in a deuterium ice layer.

$\phi_\ell = 5 \times 10^{13}$ W/cm^2, t$_{pulse}$ = 100 ps.

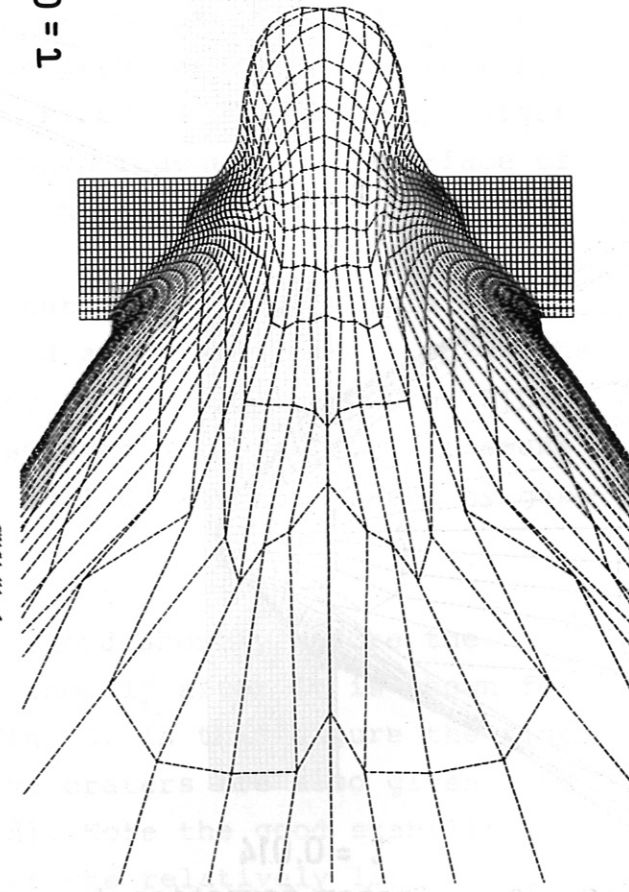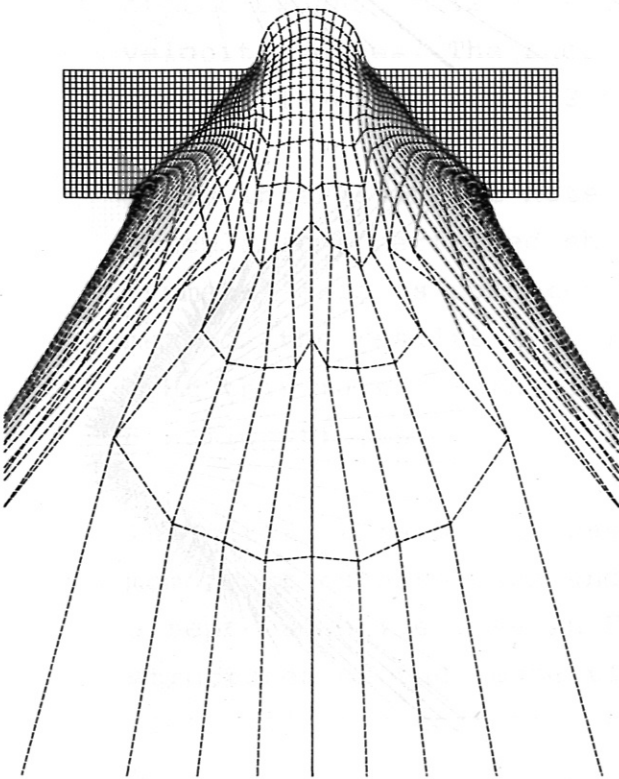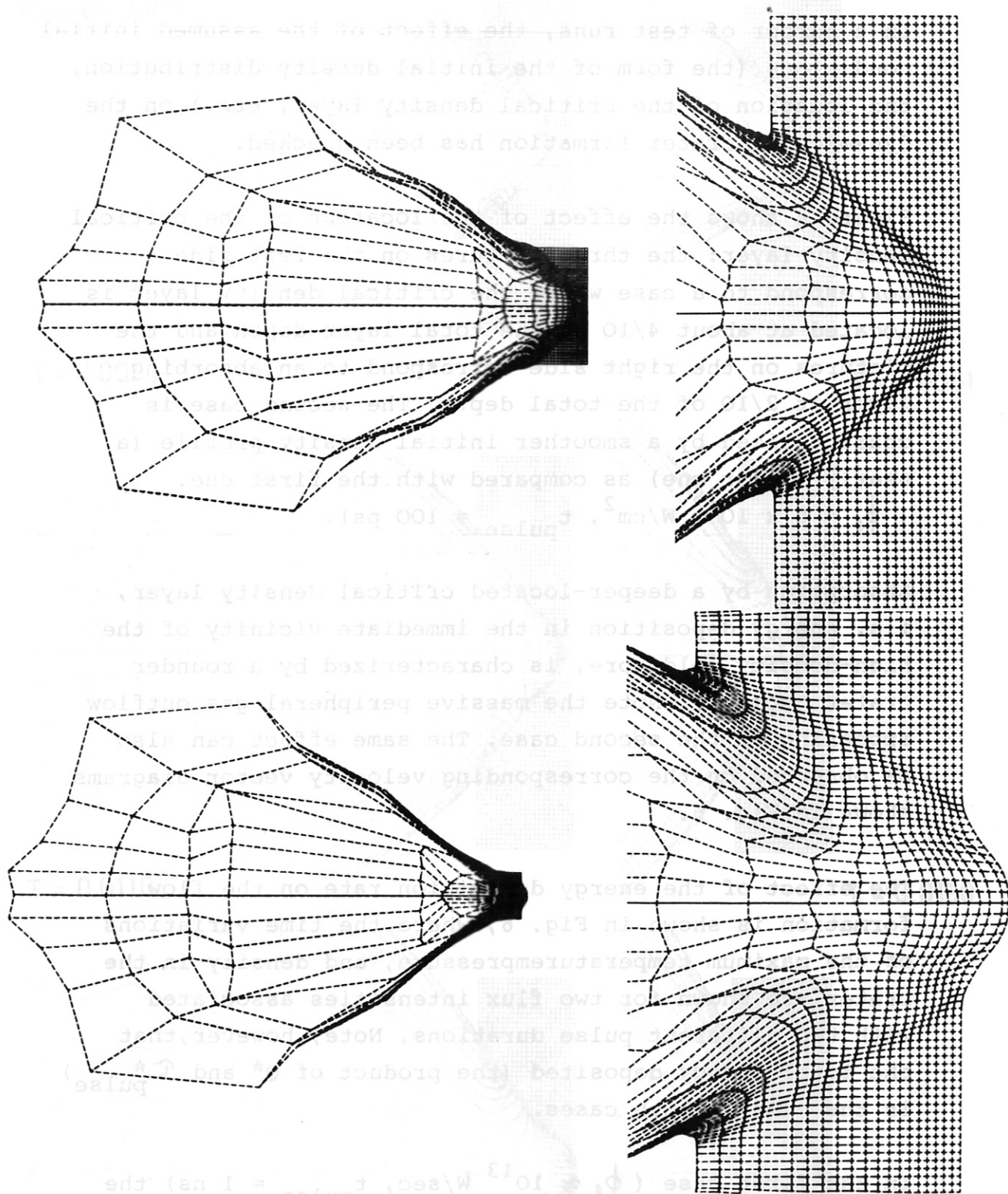(Q, τ - dimensionless quantities, τ_0 = 100 ns).

τ = 0.039

τ = 0.081

Fig. 2b   Burn-through of the deuterium
ice layer shown in Fig. 2a.

Fig. 3   The size of the expanding gas cloud
relative to the thickness of the
deuterium ice layer. The fine structure
of the developing crater is shown on
the right side.

In a number of test runs, the effect of the assumed initial conditions (the form of the initial density distribution, the location of the critical density layer, etc.) on the dynamics of crater formation has been checked.

Figure 4 shows the effect of the location of the critical density layer: the three pictures on the left side correspond to a case where the critical density layer is located at about 4/10 of the total layer depth and the pictures on the right side correspond to an absorbing layer at 2/10 of the total depth. The second case is characterized by a smoother initial density profile (a nearly linear one) as compared with the first one. (ϕ_l = 5 x 10^{13} W/cm^2, t_{pulse} = 100 ps).

Absorption by a deeper-located critical density layer, i.e. energy deposition in the immediate vicinity of the high-density cold core, is characterized by a rounder crater geometry. Note the massive peripheral gas outflow appearing in the second case. The same effect can also be observed on the corresponding velocity vector diagrams shown in Fig. 5.

The effect of the energy deposition rate on the flow formation is shown in Fig. 6, where the time variations of the maximum temperaturempressure, and density in the crater are shown for two flux intensities associated with two different pulse durations. Note, however,that the total energy deposited (the product of Q^* and τ^*_{pulse}) is the same in both cases.

In the first case ($\phi_l \approx 10^{13}$ W/sec, t_{pulse} = 1 ns) the cell deformation is relatively small during the pulse time, and the temperature and pressure maxima coincide with the cutoff moment of the laser pulse. The compression lags considerably behind the pressure rise (density change is associated with cell deformation). The density build-up signalizes shock wave formation.

$Q = 4 \times 10^7$

$\tau_{\text{pulse}} = 0.001$

$\tau = 0.0053$

$\tau = 0.0061$

$\tau = 0.0110$

$\tau = 0.0150$

$\tau = 0.0160$

$\tau = 0.0350$

<u>Fig. 4</u> Effect of the location of the absorbing layer
on the form of the crater. Left: absorption
at the surface of the dense core, right:
absorption in a layer close to the vacuum
surface.
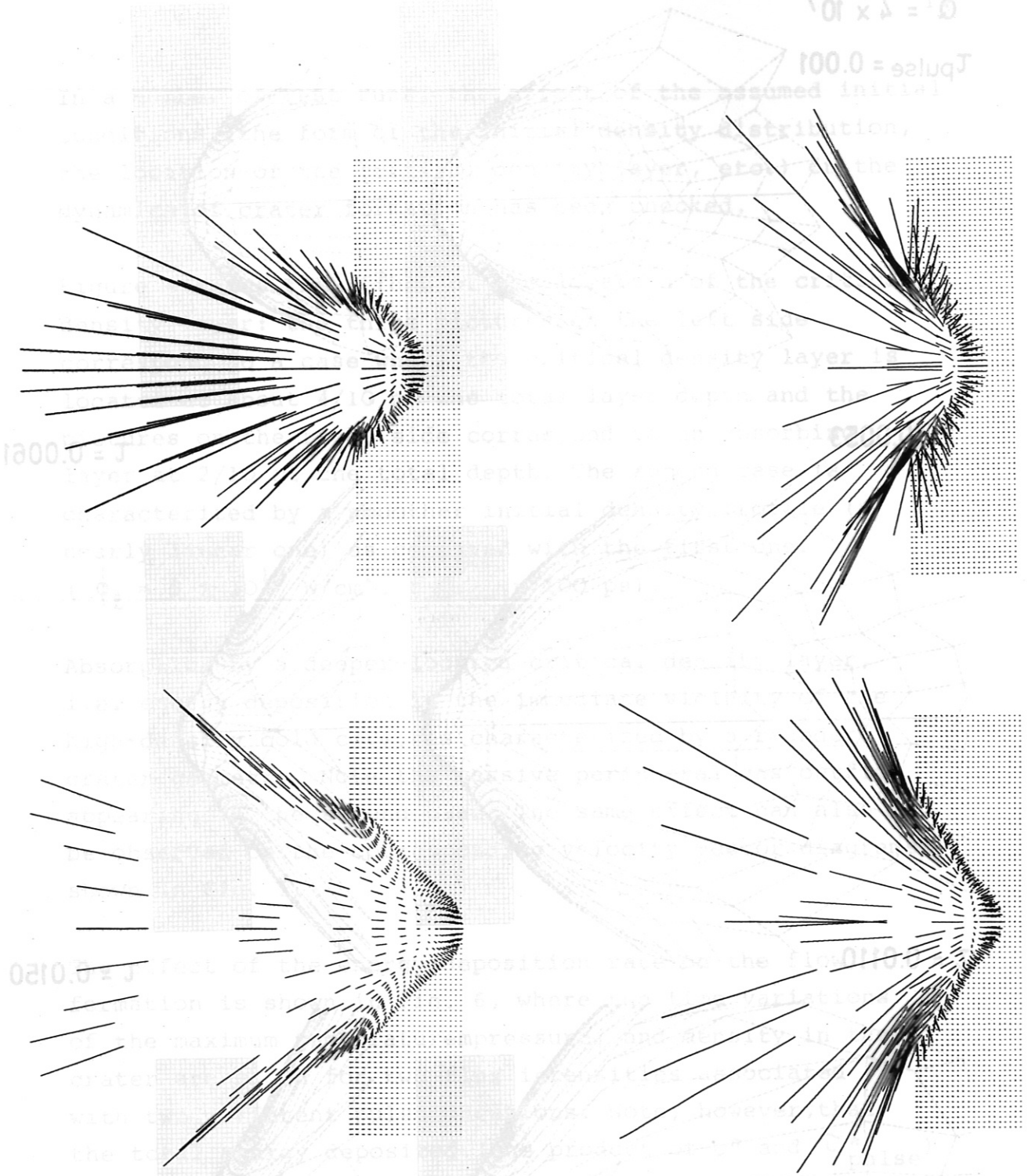
Fig. 5   Effect of the location of the absorbing
layer on the velocity vector distribution.
Left: absorption at the surface of the
dense core, right: absorption in a layer
close to the vacuum surface.

In the second case ($\phi_l \approx 10^{12}$ W/sec, t_{pulse} = 10 ns)
notable gasdynamic motion (i.e. cell deformation) sets
on before the end of the laser pulse. The peak
temperature and pressure values start to decrease
before the laser pulse is cut-off. The temperature
maximum reached is considerably lower than that in the
previous case. There is no time delay between pressure
change and density build-up.

In both cases, as soon as the shock wave formation has
been completed, the density increase behind the flat part
of the shock wave is in exact correspondence with the
Rankine-Hugoniot value as long as the shock wave motion
remains quasi-stationary. In this quasi-stationary phase,
the pressure decays exponentially with time. The
exponent characterizing the pressure decay is in good
agreement with the analytical value given for spherical
explosion waves (= 1.2).

The relation between the assumed laser flux intensity
and the peak temperature value obtained in the crater
is shown in Table 1 for two pulse durations τ_0 = 1 μs,
Q^* = 4 x 10^5 corresponds to ϕ_l = 5 x 10^{11} W/cm^2). As
can be seen, in the case of short pulses, where the
effect of gasdynamic motion is negligible for the
duration of the laser pulse, the temperature peak varies
in almost direct proportion to the flux intensity.

In the case of longer pulses characterized by the
onset of gasdynamic motion before the pulse end the
exponent of the temperature variation reduces to about
0.67.

It can readily be shown (see, for example, the
dimensional analysis performed by Bobin [17]) that the
analytical value of the exponent relating the temperature
to the laser flux intensity is 2/3 if only heat input
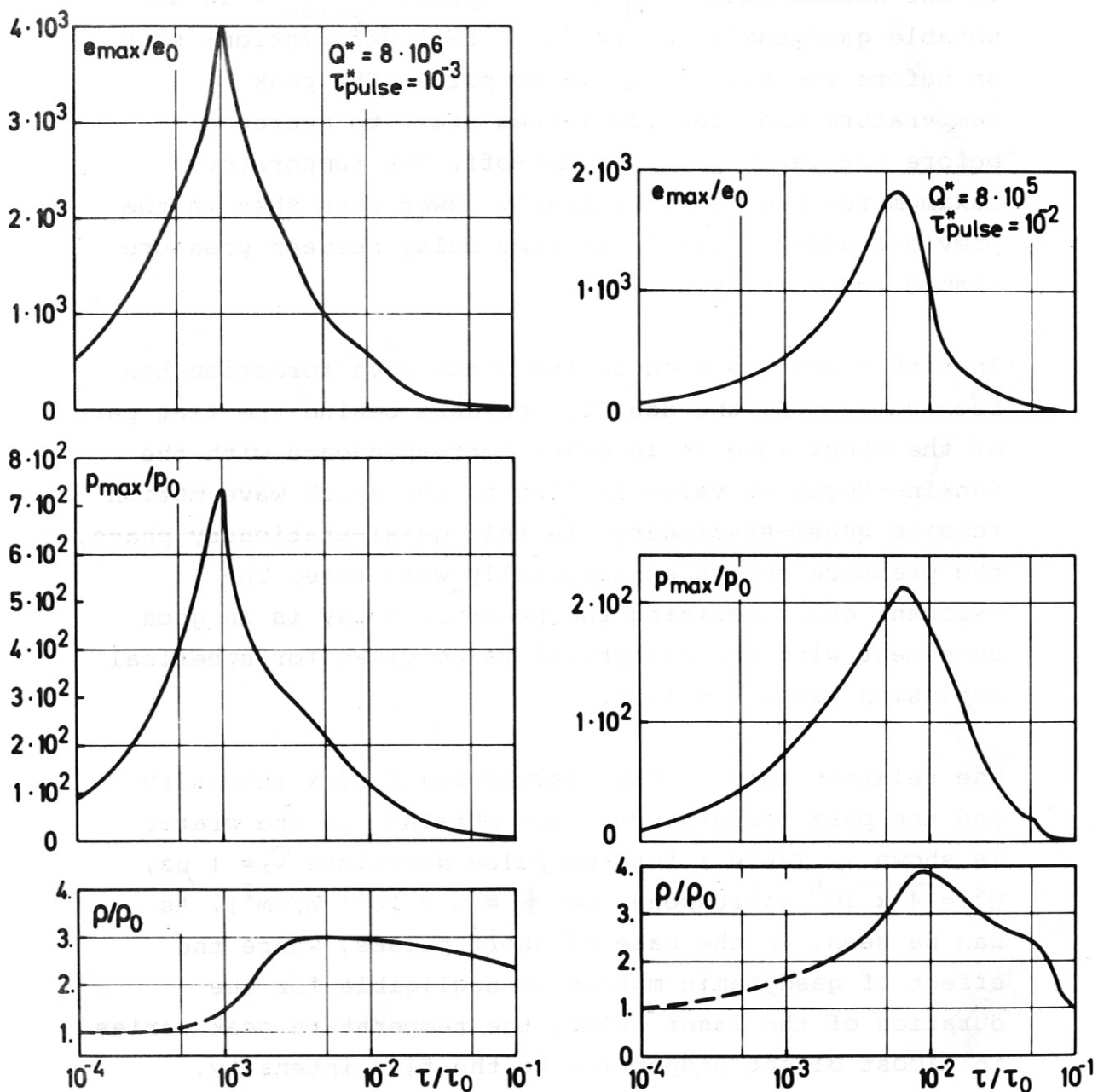and gadynamic expansion are taken into account.

Fig. 6   Effect of pulse duration (by constant laser
          energy) on the build-up of shock waves and
          on the expansion dynamics ($\phi_l \cdot t_{pulse} =$
          10^4 J/cm^2 for both cases).

T A B L E   1

TEMPERATURE PEAK OBSERVED IN THE CRATER AS A FUNCTION
OF THE LASER FLUX INTENSITY FOR TWO DIFFERENT PULSE
LENGTHS.

$$\exp \equiv \ln (e_2^* / e_1^*)_{\text{peak}} / \ln (Q^* / Q_1^*)$$

τ^*	Q^*	e^*	exp
	4×10^5	2.10×10^2	
			0.9829
10^{-3}	8×10^6	3.99×10^3	
			0.9875
	2×10^7	9.86×10^3	
			0.9023
	4×10^7	1.84×10^4	
	4×10^5	1.16×10^3	
			0.6633
10^{-2}	8×10^5	1.84×10^3	
			0.6674
	1×10^6	2.13×10^4	
			0.6665
	4×10^6	5.37×10^4	

REFERENCES

[1] R.E. Kidder and W.S. Barnes, WAZER a one-dimensional, two-temperature hydrodynamic code, Lawrence Rad. Lab., Univ. of Calif., Livermore, Rept. TID-4500, UC-34

[2] J.S. Clarke, H.N. Fisher, and R.J. Mason, Laser-driven implosion of spherical DT targets to thermonuclear burn conditions, Phys. Rev. Letters 30, No. 3, pp. 89-92 (1973)

[3] J.P. Christiansen, D. Ashby, and K.V. Roberts, MEDUSA a one-dimensional laser fusion code, Culham Lab., Preprint No. CLM-P374 (1973)

[4] E.B. Goldman, Numerical modeling of laser produced plasmas: the dynamics and neutron production in dense spherically symmetric palsmas, Plasma Physics 15, pp. 289-310 (1973)

[5] L. Lengyel, The question of laser wavelength for filling magnetic confinement machines with laser produced plasmas, Max-Planck-Inst. für Plasmaphysik, 8046 Garching, Rept. 4/131 (July 1975)

[6] P. Mulser, R. Sigel, and S. Witkowski, Plasma production by laser, Phys. Repts. 6C, No. 3 (Jan. 1973)

[7] J.H. Nuckolls, Laser induced implosion and thermonuclear burn in Laser Interaction and Related Plasma Phenomena, edited by H.J. Schwarz and H. Hora, Vol. 3B, pp. 399-425, Plenum Press, N.Y. 1974

[8] G.B. Zimmerman, Hydroynamic instabilities in laser fusion targets, Proc. Fuji Seminar on Laser Interaction with Plasma Lake Yamanaka, Nov. 1974

[9]   K.A. Brueckner, Theory and experiment in laser
        driven fusion, in Laser Interaction and Related
        Plasma Phenomena, edited by H.J. Schwarz, Vol. 3B (1974)

[10]   J.S. Clarke, Hydrogen foil penetration, Univ. Calif.,
        Los Alamos Sci. Lab., Memo No. 12-15-71

[11]   I.R. Lindemuth, The alternating-direction implicit
        numerical solution of time-dependent, two-dimensional,
        two fluid MHD equations, Univ. Calif, LLL, Rept. No.
        UCRL-51103 (1971)

[12]   L.L. Lengyel, A two-dimensional code for laser heating
        and compression calculations, 7th European Conference
        on Plasma Production by High Power Lasers, Garching,
        April 1974

[13]   W.D. Schulz, Two-dimensional Lagrangean hydrodynamic
        difference equations, Meth. Coup. Phys. $\underline{3}$, pp. 1-46,
        Academic Press, 1964

[14]   R.D. Richtmyer and K.W. Morton, Difference Methods
        for Initial-Value Problems, Intersci. Publ., N.Y. 1967

[15]   R. Wanner and H. Meyer, Sound velocity in solid
        hydrogen and deuterium, Phys. Lett. $\underline{41A}$, No. 3,
        pp. 189-190 (1972)

[16]   L.L. Lengyel and M. Salvat, Applicability of the
        uniformly expanding universe model to laser produced
        plasmas (to be published).

[17]   J.L. Bobin, Flame propagation and overdense heating
        in a laser created plasma. Phys. Fluids $\underline{14}$, No. 11,
        pp. 2341-2354 (1971)